

A review on 3d transition metal dilute magnetic $RE\text{In}_3$ intermetallic compounds

Xin-Peng Guo(郭新鹏), Yong-Quan Guo(郭永权), Lin-Han Yin(殷林瀚), and Qiang He(何强)
Citation: Chin. Phys. B, 2022, 31 (**3**): 037501. DOI: 10.1088/1674-1056/ac20cd
Journal homepage: http://cpb.iphy.ac.cn; http://iopscience.iop.org/cpb
What follows is a list of articles you may be interested in

Magnetic phase diagram of single-layer $CrBr_3$

Wei Jiang(江伟), Yue-Fei Hou(侯跃飞), Shujing Li(李淑静), Zhen-Guo Fu(付振国), and Ping Zhang(张平)
Chin. Phys. B, 2021, 30 (**12**): 127501. DOI: 10.1088/1674-1056/ac0043

Ground-state phase diagram of the dimerizedspin-1/2 two-leg ladder

Cong Fu(傅聪), Hui Zhao(赵晖), Yu-Guang Chen(陈宇光), and Yong-Hong Yan(鄢永红)
Chin. Phys. B, 2021, 30 (**8**): 087501. DOI: 10.1088/1674-1056/abec31

Emergent O(4) symmetry at the phase transition from plaquette-singlet to antiferromagnetic order in quasi-two-dimensional quantum magnets

Guangyu Sun(孙光宇), Nvsen Ma(马女森), Bowen Zhao(赵博文), Anders W. Sandvik, and Zi Yang Meng(孟子杨)
Chin. Phys. B, 2021, 30 (**6**): 067505. DOI: 10.1088/1674-1056/abf3b8

Powder x-ray diffraction and Rietveld analysis of $(C_2H_5NH_3)_2CuCl_4$

Yi Liu(刘义), Jun Shen(沈俊), Zunming Lu(卢遵铭), Baogen Shen(沈保根), and Liqin Yan(闫丽琴)
Chin. Phys. B, 2021, 30 (**6**): 067502. DOI: 10.1088/1674-1056/abee0a

Absence of magnetic order in dichloro [1,2-bis (diphenylphosphino) ethane] nickel^{2+} single crystal

Shuaiqi Ma(马帅奇), Linlin An(安琳琳), and Xiangde Zhu(朱相德)
Chin. Phys. B, 2021, 30 (**5**): 057501. DOI: 10.1088/1674-1056/abe233

REVIEW

A review on 3d transition metal dilute magnetic $RE\text{In}_3$ intermetallic compounds

Xin-Peng Guo(郭新鹏), Yong-Quan Guo(郭永权)[†], Lin-Han Yin(殷林瀚), and Qiang He(何强)

School of Energy Power and Mechanical Engineering, North China Electric Power University, Beijing 102206, *China*

(Received 22 June 2021; revised manuscript received 22 August 2021; accepted manuscript online 25 August 2021)

The dilute magnetic intermetallic compound (DMIC) is an extended study of the dilute magnetic semiconductor. The giant magnetic effect and room temperature ferromagnetism are induced by doping minor 3d transition metal into $RE\text{In}_3$ intermetallic compound. Owing to the metallic processability, the $RE\text{In}_3$-based DMIC might have the potential application as magnetoelectric device. In this review, the structural stability, magnetic and electric transport properties of $RE\text{In}_{3-x}T_x$ (RE = rare earth; T = Co, Mn, Fe; x = 0–0.3) have been systematically summarized and analyzed.

Keywords: dilute magnetic intermetallic compounds, phase transition, magnetic properties, magnetic transport

PACS: 75.50.–y, 61.50.–f, 61.66.Dk, 75.30.Hx **DOI:** 10.1088/1674-1056/ac20cd

1. Introduction

Over the last decades, the magnetic semiconductors have received much attention due to their potential application on spin-electronic devices by spin modulating electric transport.[1] According to the content of magnetic elements in semiconductor, two kinds of magnetic semiconductors are classified, which correspond to the concentrated magnetic semiconductor (CMS) and dilute magnetic semiconductor (DMS). The early study is mainly focused on EuX (X = O, Se) and $CdCr_2X_4$ (X = S, Se) CMSs due to their unique ferromagnetic semiconductor characteristics.[2–5] Owing to the ferromagnetism in CMS, the band gap shows the red shift, which causes the exchange interaction between itinerant electrons and localized magnetic spins. However, the further development and application of CMS are restricted by their low Curie temperatures and complex preparation process.[6] Thus, the attention is changed to the magnetic atom/ion-doped III–V, II–VI, IV–IV, and II–II–V group semiconductors.[7–15] The dilute magnetic semiconductor, which is formed by substituting minor magnetic ions for non-magnetic ions, has attracted much attention due to its excellent magnetic transport properties. In recent years, the novel chalcopyrite-based DMSs have been widely studied.[16] The room temperature ferromagnetism has been obtained in $Cd_{1-x}Mn_xGeP_2$, $CuIn_{1-x}Co_xTe_2$, and Cr-doped $CuZnSe_2$.[17–19] The ferromagnetism is suggested to originate from the spin–spin interactions of 3d transition metal.[19] The codoping of Co and Ce into $CuInTe_2$ induces the room temperature ferromagnetism. The magnetization of $CuIn_{0.9}Ce_xCo_{0.1-x}Te_2$ is enhanced, which is ascribed to the exchanging interaction between 4f electron of Ce and 3d electron of Co. The high doping ratio of Co and Ce is beneficial for increasing saturation magnetization.[20] Mn-doped $CuInSe_2$ semiconductors show antiferromagnetic order with very low Néel temperature.[21–23] $CuIn_{1-x}Co_xSe_2$ shows the superparamagnetism at room temperature.[24]

In recent years, the interest has been growing in the rare earth-indium ($RE\text{In}_3$) compounds with a cubic $AuCu_3$-type crystal structure.[25–27] $RE\text{In}_3$ shows remarkable features, such as heavy fermion, antiferromagnetism, superconductivity at critical temperature or pressure, crystal field effects, Kondo effect, and multiaxial magnetic structures.[25,27–34] $CeIn_3$ belongs to a heavy fermion and shows unique magnetic and electric properties such as antiferromagnetic order at 10 K, superconductivity under applied high pressure, and Kondo effect.[35] $GdIn_3$ orders antiferromagnetically at 45 K, which is the highest Néel temperature among the $RE\text{In}_3$ intermetallic compounds.[36] The crystal electrical-field (CEF) ground state is a singlet for the $PrIn_3$ intermetallic compound, its low-temperature susceptibility is almost temperature-independent, but inversely proportional to the splitting energy of the excited states. The two electrons in the unfilled 4f shell of the Pr ions form a multiplet with $J = 4$, giving rise to a magnetic moment of $\mu_B gJ$ with $g = 0.8$. A remarkable feature of $PrIn_3$ is a large nuclear quadrupole interaction ($e^2qQ/h = +228$ MHz) at In site.[37,38] $NdIn_3$ is a typical 4f-localized intermetallic compound with a Néel temperature below 5.9 K. With the increasing external magnetic field, the magnetic transformation from the antiferromagnetic to paramagnetic occurs.[39] $HoIn_3$ orders antiferromagnetically at 10.5 K and its magnetic structure is suggested to be multiaxial. The potential application of $HoIn_3$ as a regenerator material is also expected since its abnormal heat capacity is associated with the antiferromagnetic

[†]Corresponding author. E-mail: yqguo@ncepu.edu.cn

© 2022 Chinese Physical Society and IOP Publishing Ltd

transition in the temperature range of 4 K–10 K.[40]

The dilute magnetic intermetallic compounds (DMIC) can be obtained by doping minor 3d transition metal (Co, Mn or Fe) into intermetallics.[41,42] Mn-doped $EuMn_{0.3}Ga_{2.7}$ orders ferromagnetically at room temperature under applying a low field of 40 Oe (1 Oe = 79.5775 A/m).[43] As for the dilute magnetic $RE\text{In}_3$, the studies mainly focus on the doping effects on the structure and magnetic properties at In site or *RE* site.[31,44,45] It is well known that the 3d transition metals play an important role in magnetic materials due to their significant contributions to the magnetization and magnetic anisotropy by coupling with 4f electrons of the rare-earth.[46] Since the pure Co is strongly ferromagnetic, it is expected to improve the magnetic property of $RE\text{In}_3$ by doping minor Co. Doping of Co into $RE\text{In}_3$ (RE = Pr, Nd,) induces a giant magnetic effect with Curie temperature more than room temperature.[36,38] The giant moment originates from the partial substitution of non-magnetic element In by magnetic element Co in the host material, and thus, a net moment is produced. The ferromagnetism is caused by the spin–spin interactions between Co and Co or Co and *RE*.

The objective of this paper is to introduce a brief review on minor doping of 3d transition metal T into $RE\text{In}_3$ intermetallic compounds (RE = Pr, Nd, Gd, Ho; T = Co, Mn, and Fe). The transition of the structure and magnetic properties of $RE\text{In}_{3-x}T_x$ have been systematically discussed.

2. Structural stability

As shown in Fig. 1,[36,38,47–51] all the $RE\text{In}_3$ alloys are single phase with a cubic $AuCu_3$-type structure. The cubic structure is still stable by doping minor 3d transition metal into $RE\text{In}_3$. The single-phase region corresponds to $RE\text{In}_{3x}\text{Mn}_x$ with $x < 0.3$ and $RE\text{In}_{3-x}\text{Co}_x$ with $x \leq 0.1$. However, the structural stability of cubic phase reduces with doping minor Fe into $RE\text{In}_3$.[47] The additional satellite peaks can be observed out of solid solution region of $RE\text{In}_{3-x}\text{Co}_x$. The satellite peaks can be indexed with a hexagonal $CaIn_2$-type or $GaGd_2$-type structure based on the structural refinement.[36,38,48,52] In element is detected out of $RE\text{In}_{3-x}\text{Mn}_x$ solid solution.[49] Doping minor Fe into $RE\text{In}_3$ induces the decomposition of the cubic phase, and In is separated from $RE\text{In}_3$. With increasing Fe doping content, the metaphase is observed and its structural formula is suggested to be $RE(\text{In, Fe})_2$.[48]

The crystallographic parameters of $RE\text{In}_{3-x}T_x$ are summarized in Table 1.[36,38,47–53] According to the structural refinements, the main phase of $RE\text{In}_{3-x}T_x$ crystallizes into a cubic $AuCu_3$-type structure with a space group of $Pm\bar{3}m$ (as shown in Fig. 2[52]). Two kinds of non-equivalent crystal positions are included in one unit cell. The atomic occupations correspond to the 1*a* (0, 0, 0) site for *RE* atoms, and the 3*c* (1/2, 1/2, 0) site for In and transition metal Co, Mn or Fe atoms.

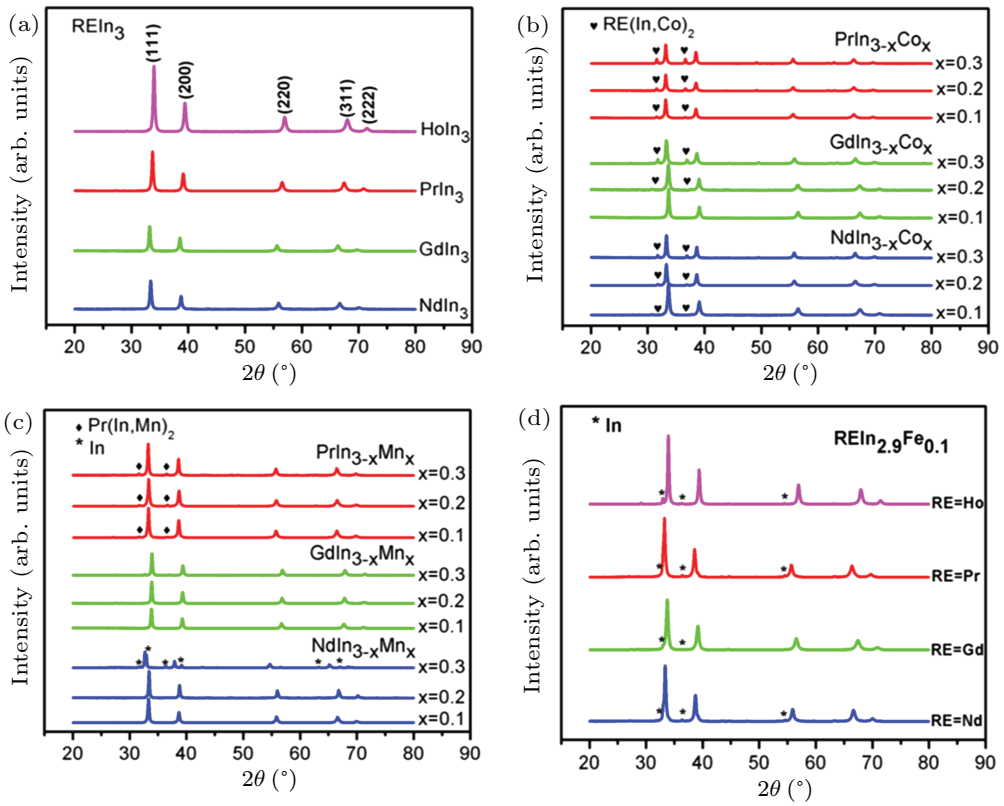


Fig. 1. XRD patterns of $RE\text{In}_{3-x}T_x$ intermetallic compounds: (a) $RE\text{In}_3$; (b) $RE\text{In}_{3-x}\text{Co}_x$; (c) $RE\text{In}_{3-x}\text{Mn}_x$; (d) $RE\text{In}_{2.9}\text{Fe}_{0.1}$. The figures are adapted from Refs. [36,38,47–51].

Table 1. The crystal structure for $RE\text{In}_{3-x}T_x$ alloys.

Formula	Symmetry	Structure	Ref.
$PrIn_3$	cub	$AuCu_3$	[38]
$PrIn_{2.9}Co_{0.1}$	cub + hcp	$AuCu_3 + CaIn_2$	[38]
$PrIn_{2.8}Co_{0.2}$	cub + hcp	$AuCu_3 + CaIn_2$	[38]
$PrIn_{2.7}Co_{0.3}$	cub + hcp	$AuCu_3 + CaIn_2$	[38]
$NdIn_3$	cub	$AuCu_3$	[36]
$NdIn_{2.9}Co_{0.1}$	cub + hcp	$AuCu_3 + CaIn_2$	[36]
$NdIn_{2.8}Co_{0.2}$	cub + hcp	$AuCu_3 + CaIn_2$	[36]
$NdIn_{2.7}Co_{0.3}$	cub + hcp	$AuCu_3 + CaIn_2$	[36]
$GdIn_3$	cub	$AuCu_3$	[48]
$GdIn_{2.9}Co_{0.1}$	cub	$AuCu_3$	[48]
$GdIn_{2.8}Co_{0.2}$	cub + hcp	$AuCu_3 + GdGa_2$	[48]
$GdIn_{2.7}Co_{0.3}$	cub + hcp	$AuCu_3 + GdGa_2$	[48]
$HoIn_3$	cub	$AuCu_3$	[52]
$HoIn_{2.9}Co_{0.1}$	cub	$AuCu_3$	[51]
$HoIn_{2.4}Co_{0.6}$	cub + ort		[52]
$HoIn_{1.5}Co_{1.5}$	cub + ort		[52]
$HoIn_{0.6}Co_{2.4}$	ort + rho		[52]
$PrIn_{2.9}Mn_{0.1}$	cub + hcp	$AuCu_3 + GdGa_2$	[48]
$PrIn_{2.8}Mn_{0.2}$	cub + hcp	$AuCu_3 + GdGa_2$	[48]
$PrIn_{2.7}Mn_{0.3}$	cub + hcp	$AuCu_3 + GdGa_2$	[48]
$NdIn_{2.9}Mn_{0.1}$	cub	$AuCu_3$	[49]
$NdIn_{2.8}Mn_{0.2}$	cub	$AuCu_3$	[49]
$NdIn_{2.7}Mn_{0.3}$	cub + tet	$AuCu_3 + In$	[49]
$GdIn_{2.9}Mn_{0.1}$	cub	$AuCu_3$	[50]
$GdIn_{2.8}Mn_{0.2}$	cub	$AuCu_3$	[50]
$GdIn_{2.7}Mn_{0.3}$	cub	$AuCu_3$	[50]
$PrIn_{2.9}Fe_{0.1}$	cub + tet	$AuCu_3 + In$	[47]
$NdIn_{2.9}Fe_{0.1}$	cub + tet	$AuCu_3 + In$	[47]
$GdIn_{2.9}Fe_{0.1}$	cub + tet	$AuCu_3 + In$	[47]
$GdIn_{2.7}Fe_{0.3}$	cub + tet	$AuCu_3 + In$	[48]
$HoIn_{2.9}Fe_{0.1}$	cub + tet	$AuCu_3 + In$	[47]

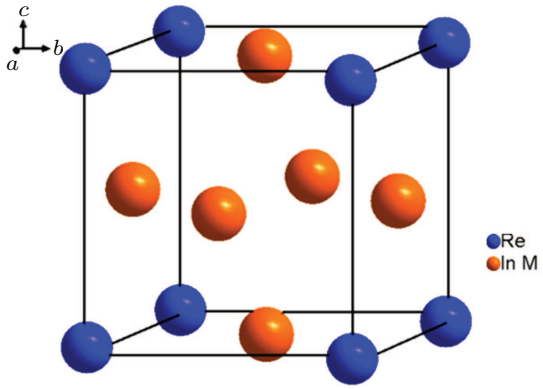


Fig. 2. The structural frame of cubic $RE\text{In}_{3-x}T_x$. The figure is adapted from Ref. [52].

The structure of the metaphase is suggested as an isomorphic structure of $CaIn_2$ with a space group of $P6_3/mmc$, $Z = 2$ and $GdGa_2$ with a space group of $P6/mmm$, $Z = 1$. There are two non-equivalent crystal positions in a unit cell with $CaIn_2$-type isomorphic structure, *i.e.*, $2b$ (0, 0, 1/4) and $4f$ (1/3, 2/3, z) crystal positions, which are occupied by $2RE$ and 4(In, T) atoms, respectively. For $GdGa_2$-type structure, the atomic occupations correspond to $1a$ (0, 0, 0) site for RE atoms and $2d$ (1/3, 2/3, 1/2) site for In and T atoms, respectively. The lattice parameters of the main- and meta-phases are summarized in Tables 2 and 3.[47–50,52,53]

Table 2. The lattice parameters of the main phase in $RE\text{In}_{3-x}T_x$.

Formula	Space group	Lattice parameter a (Å)				Ref.
		$x = 0$	$x = 0.1$	$x = 0.2$	$x = 0.3$	
$PrIn_{3-x}Co_x$	$Pm\bar{3}m$	4.669(0)	4.670(1)	4.670(5)	4.673(3)	[38]
$NdIn_{3-x}Co_x$	$Pm\bar{3}m$	4.648(1)	4.655(3)	4.657(5)	4.654(7)	[36]
$GdIn_{3-x}Co_x$	$Pm\bar{3}m$	4.6065(00)	4.6058(02)	4.6052(02)	4.6052(21)	[48]
$NdSn_{3-x}Co_x$	$Pm\bar{3}m$	4.685(3)	4.683(2)	4.680(7)	4.680(1)	[53]
$SmSn_{3-x}Co_x$	$Pm\bar{3}m$	4.779(3)	4.773(2)	4.762(7)	4.758(3)	[53]
$PrIn_{3-x}Mn_x$	$Pm\bar{3}m$	4.6715(01)	4.6678(01)	4.6654(01)	4.6642(01)	[48]
$NdIn_{3-x}Mn_x$	$Pm\bar{3}m$	4.741(3)	4.738(3)	4.650(2)	4.641(5)	[49]
$GdIn_{3-x}Mn_x$	$Pm\bar{3}m$	4.605(4)	4.597(0)	4.589(3)	4.580(0)	[50]
$PrIn_{3-x}Fe_x$	$Pm\bar{3}m$	4.674(6)	4.671(5)			[47]
$NdIn_{3-x}Fe_x$	$Pm\bar{3}m$	4.659(0)	4.658(0)			[47]
$GdIn_{3-x}Fe_x$	$Pm\bar{3}m$	4.608(1)	4.606(3)			[47]
$HoIn_{3-x}Fe_x$	$Pm\bar{3}m$	4.569(4)	4.568(0)			[47]

Table 3. The lattice parameters of the metaphase in $RE\text{In}_{2-x}T_x$.

Formula	Space group	Lattice parameter (Å)	$x = 0.1$	$x = 0.2$	$x = 0.3$	Ref.
$PrIn_{2-x}Co_x$	$P6_3/mmc$	a	4.898(1)	4.899(5)	4.902(3)	[38]
		c	7.600(5)	7.598(3)	7.592(3)	
$NdIn_{2-x}Co_x$	$P6_3/mmc$	a	4.868(5)	4.868(6)	4.902(3)	[36]
		c	7.547(5)	7.555(3)	7.557(8)	
$GdIn_{2-x}Co_x$	$P6/mmm$	a		4.7695(21)	4.7731(36)	[48]
		c		4.0738(09)	4.0633(13)	
$PrIn_{2-x}Mn_x$	$P6/mmm$	a	4.8898(16)	4.9129(07)	4.9101(05)	[48]
		c	3.4728(08)	3.7808(05)	3.7800(03)	

Since the pure binary $RE\text{In}_2$ does not exist naturally, $RE\text{In}_{2-x}T_x$ alloy is prepared for checking its single-phase with CaIn_2- or GaGd_2-type structure. However, the phase identification confirms that the single phase $RE\text{In}_{2-x}T_x$ does not exist at all. It implies that $RE(\text{In, Co})_2$ is metaphase, which might originate from the crystal growing defect and separate from the cubic phase. The phase separation in $RE\text{In}_{3-x}\text{Co}_x$ is suspected to be driven by the lattice distortion originated from the atomic size effect. The substitution of Co for In could cause a large lattice distortion and thus induces the structural reconstruction from cubic $RE\text{In}_{3-x}\text{Co}_x$ to hexagonal $RE\text{In}_{2-x}\text{Co}_x$. The projections of two structures reveal the mechanism of phase separation from the cubic $RE\text{In}_3$ to hexagonal $RE\text{In}_{2-x}\text{Co}_x$. The reconstruction originates from the rotation of (In, Co)6 hexagonal ring, comparing to the projection of cubic $RE\text{In}_3$ along [111] direction, the structural skeleton of $RE(\text{In, Co})_2$ could be formed by rotating the (In, Co)6 hexagonal ring with an angle of 30° along [111] direction, as shown in Fig. 3.[36]

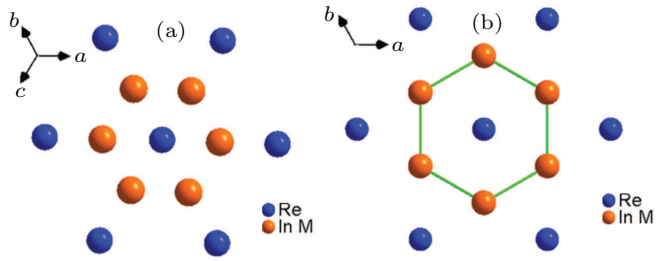


Fig. 3. The projection of cubic phase along [111] direction in $RE\text{In}_3$ and hexagonal phase along [001] direction in $RE(\text{In, Co})_2$. The figures are adapted from Ref. [36].

The atomic size can directly influence the crystal structures of materials. The phase transition and lattice distortion in $RE\text{In}_{3-x}T_x$ might be driven by the atomic size effect. Since the atomic radii of Co (1.25 Å), Mn (1.32 Å), and Fe (1.24 Å) are quite different from that of In (1.66 Å) or rare-earth atoms (more than 1.74 Å). The doping of Co, Mn or Fe induces large lattice distortion.

In order to discuss the effect of atomic size on the structural stability of $RE\text{In}_{3-x}T_x$ cubic phase, the effective atomic radius ratio is defined between *RE* and (In, Co), *RE* and (In, Mn), as well as *RE* and (In, Fe).[47]

The effective atomic radius ratio equation of $RE\text{In}_3$ is

$$\bar{R} = r_{\text{R}}/r_{\text{In}}, \tag{1}$$

where r_{R} and r_{In} are the atomic radii of *RE* and In, respectively. The range of $\bar{R}$ is from 1.08 to 1.10.

The effective atomic radius ratio equation of $RE\text{In}_{3-x}M_x$ is

$$R_{\text{A}} = \frac{r_{\text{R}}}{\langle r_{\text{In},M}\rangle}, \tag{2}$$

where

$$\langle r_{\text{In},M}\rangle = \frac{(3-x)\cdot r_{\text{In}} + x\cdot r_M}{3}, \tag{3}$$

R_{A}, r_{R}, $\langle r_{\text{In},M}\rangle$ are the effective atomic radius ratio, the atomic radius of *RE*, and the average atomic radius of In and transition metal (Co, Mn or Fe) respectively.

Table 4 shows the effective atomic radius ratio of $RE\text{In}_{3-x}M_x$ compounds.[47–52] It implies that the cubic phase can be stabilized in $R_{\text{A}} < 1.09$ for $RE\text{In}_{3-x}\text{Co}_x$ and $R_{\text{A}} < 1.10$ for $RE\text{In}_{3-x}\text{Mn}_x$, respectively.

The electro-negativity difference between (In, *M*) and rare earth is also considered as a correlative criterion for the structural stability of the cubic phase. It is defined for $RE\text{In}_3$

$$\Delta X_0 = X_{\text{In}} - X_{RE}. \tag{4}$$

The electro-negativity difference equation of $RE\text{In}_{3-x}M_x$ is

$$\Delta X = \frac{(3-x)\cdot X_{\text{In}} + x\cdot X_M}{3} - X_{RE}, \tag{5}$$

where X_{In}, X_{RE}, and X_M are corresponding to the electro-negativity of In, rare earth, and 3d transition metal, respectively.

The calculated electro-negativity differences show that the cubic phase ΔX ranging from 0.384 to 0.397 for $RE\text{In}_{3-x}\text{Co}_x$ and from 0.387 to 0.424 for $RE\text{In}_{3-x}\text{Mn}_x$, as listed in Table 5.[47–52]

Table 4. The effective atomic radius ratios of $RE\text{In}_{3-x}T_x$ alloys.

	$r_{\text{In}} = 1.66$ Å, $r_{\text{Co}} = 1.25$ Å, $r_{\text{Mn}} = 1.32$ Å, $r_{\text{Fe}} = 1.24$ Å									
	Elements	r_{R}	$\langle r_{\text{In,Co}}\rangle$	$R_{\text{A}_{\text{Co}}}$	Ref.	$\langle r_{\text{In,Mn}}\rangle$	$R_{\text{A}_{\text{Mn}}}$	Ref.	$\langle r_{\text{In,Fe}}\rangle$	$R_{\text{A}_{\text{Fe}}}$	Ref.
$x = 0.1$	Pr	1.82	1.646	1.106	[38]	1.649	1.104	[48]	1.646	1.106	[47]
	Nd	1.81		1.100	[36]		1.098	[49]		1.100	[47]
	Gd	1.79		1.087	[48]		1.086	[50]		1.087	[47]
	Ho	1.76		1.069	[54]					1.069	[47]
$x = 0.2$	Pr	1.82	1.633	1.115	[38]	1.637	1.112	[48]			
	Nd	1.81		1.108	[36]		1.106	[49]			
	Gd	1.79		1.096	[48]		1.093	[50]			
$x = 0.3$	Pr	1.82	1.619	1.124	[38]	1.626	1.119	[48]			
	Nd	1.81		1.118	[36]		1.113	[49]			
	Gd	1.79		1.106	[48]		1.101	[50]			

Table 5. The electro-negativity differences of $RE\text{In}_{3-x}T_x$ alloys.

	$X_{\text{In}} = 1.49$, $X_{\text{Co}} = 1.70$, $X_{\text{Mn}} = 1.60$, $X_{\text{Fe}} = 1.64$							
	Elements	X_{RE}	ΔX_{Co}	Ref.	ΔX_{Mn}	Ref.	ΔX_{Fe}	Ref.
$x = 0.1$	Pr	1.07	0.427	[38]	0.424	[48]	0.425	[47]
	Nd	1.07	0.427	[36]	0.424	[49]	0.425	[47]
	Gd	1.11	0.387	[48]	0.384	[50]	0.385	[47]
	Ho	1.10	0.397	[54]			0.395	[47]
$x = 0.2$	Pr	1.07	0.434	[38]	0.427	[48]		
	Nd	1.07	0.434	[36]	0.427	[49]		
	Gd	1.11	0.394	[48]	0.387	[50]		
$x = 0.3$	Pr	1.07	0.441	[38]	0.431	[48]		
	Nd	1.07	0.441	[36]	0.431	[49]		
	Gd	1.11	0.401	[48]	0.391	[50]		

3. Magnetic properties

According to the temperature dependence of magnetization, Mn-doped $\text{NdIn}_{3-x}\text{Mn}_x$ ($x < 0.3$) cubic phase shows the paramagnetic property at room temperature, however, a weak ferromagnetic property is observed out of its single-phase region.[49] The antiferromagnetic order is observed in $RE\text{In}_{3-x}T_x$ (RE = Nd, Pr, Gd; T = Mn, Co) intermetallics in low-temperature region. Mn doping into GdIn_3 causes the decrease of Néel temperature from 42.10 K to 31.66 K due to the distortion of Gd(In, Mn)$_3$ tetrahedron formed by Gd at corners and (In, Mn) at face centers in the unit cell. The formation of the antiferromagnetic ordering might originate from the exchanging interaction between the unpaired 4f electron spin of RE and the surrounding conduction electrons at low temperature.[50] $RE\text{In}_{2.9}\text{Co}_{0.1}$ (RE = Pr, Nd) shows low temperature antiferromagnetic order and room temperature ferromagnetic order with Curie temperature more than 523 K.[36,38]

Table 6. Various magnetic properties for $RE\text{In}_{3-x}T_x$ alloys.

Formula	Magnetic phase at room temperature	M_{s} (μ_{B})	χ	T_{N} (K)	T_{c} (K)	Ref.
PrIn_3	PM		0.0118			[38]
$\text{PrIn}_{2.9}\text{Co}_{0.1}$	PM + FM	0.0718	0.0103		940	[38]
$\text{PrIn}_{2.8}\text{Co}_{0.2}$	FM	0.2272		8.91–14.73	926	[38]
$\text{PrIn}_{2.7}\text{Co}_{0.3}$	FM	0.4326			948	[38]
NdIn_3	PM		0.01158	6.8–7		[36]
$\text{NdIn}_{2.9}\text{Co}_{0.1}$	PM + FM	0.0964	0.01232		524	[36]
$\text{NdIn}_{2.8}\text{Co}_{0.2}$	PM + FM	0.2237	0.01649			[36]
$\text{NdIn}_{2.7}\text{Co}_{0.3}$	FM	0.3537				[36]
GdIn_3	FM		0.05013	45–48		[48]
$\text{GdIn}_{2.9}\text{Co}_{0.1}$	PM + FM	0.0168	0.0492	45.69		[48]
$\text{GdIn}_{2.9}\text{Co}_{0.1}$	PM + FM	0.0341	0.0494			[48]
$\text{GdIn}_{2.9}\text{Co}_{0.1}$	PM + FM	0.0872	0.0429			[48]
HoIn_3	PM			11		[52]
$\text{HoIn}_{2.4}\text{Co}_{0.6}$	PM		0.10270			[52]
$\text{HoIn}_{1.5}\text{Co}_{1.5}$	PM + FM			24.68	215	[52]
$\text{HoIn}_{0.6}\text{Co}_{2.4}$	FM	0.0641	0.11596		468	[52]
$\text{PrIn}_{2.9}\text{Mn}_{0.1}$	PM		0.12572			[48]
$\text{PrIn}_{2.8}\text{Mn}_{0.2}$	PM		0.14846			[48]
$\text{PrIn}_{2.7}\text{Mn}_{0.3}$	PM		0.15920			[48]
$\text{NdIn}_{2.9}\text{Mn}_{0.1}$	PM					[49]
$\text{NdIn}_{2.7}\text{Mn}_{0.3}$	PM + FM					[49]
$\text{GdIn}_{2.9}\text{Mn}_{0.1}$	PM		0.08736	40.90		[50]
$\text{GdIn}_{2.8}\text{Mn}_{0.2}$	PM		0.09770	36.34		[50]
$\text{GdIn}_{2.7}\text{Mn}_{0.3}$	PM		0.10328	36.64		[50]
$\text{PrIn}_{2.9}\text{Fe}_{0.1}$	PM + FM	0.12781	0.00811			[47]
$\text{NdIn}_{2.9}\text{Fe}_{0.1}$	PM + FM	0.14358	0.00694			[47]
$\text{GdIn}_{2.9}\text{Fe}_{0.1}$	PM + FM	0.25148	0.05130			[47]
$\text{HoIn}_{2.9}\text{Fe}_{0.1}$	PM + FM	0.19297	0.01019			[47]

According to the studies on magnetic properties of $RE\text{In}_{3-x}T_x$,[36,38,47–50,52] the magnetic properties are summarized in Table 6. The magnetizing mechanisms of $RE\text{In}_{3-x}T_x$ are different for the various magnetic phase, Langevin model[54] is usually used in the ferromagnetic region:

$$M = N\mu\left(\coth\frac{\mu H}{k_{\rm B}T} - \frac{k_{\rm B}T}{\mu H}\right), \tag{6}$$

where M, N, μ, H, and T are corresponding to the magnetization, atomic numbers, moment, external field, and temperature. $k_{\rm B}$ is Boltzmann constant.

In the paramagnetic region, the magnetizing curves follow a linear model as given below:

$$M = \chi H, \tag{7}$$

where χ is the susceptibility.

However, Langevin model does not work for ferromagnetic $RE\text{In}_{3-x}\text{Co}_x$, a model, which is based on the original Weiss's model is introduced as follows:

$$M = M_{\rm s}\exp\left(-\frac{a}{H}\right), \tag{8}$$

where $M_{\rm s}$ is the saturation moment.

This equation could be rewritten by the Taylor series expansion algorithm as Weiss model

$$M = M_{\rm s}\left(1 - \frac{a_1}{H} + \frac{a_2}{H^2} - \frac{a_3}{H^3}\cdots\right), \tag{9}$$

where a is a parameter related to the applied external field.

In the region of the mixed ferromagnetic and paramagnetic phase, the magnetization curve follows an equation as

$$M = M_{\rm s}\exp\left(-\frac{a}{H}\right) + \chi H, \tag{10}$$

where the first and second terms are the contributions to magnetization originating from the ferromagnetic and paramagnetic phases, respectively. The magnetization curves follow the three models in ferromagnetic, paramagnetic and mixture of ferromagnetic and paramagnetic regions, as shown in Fig. 4.[36,47,48]

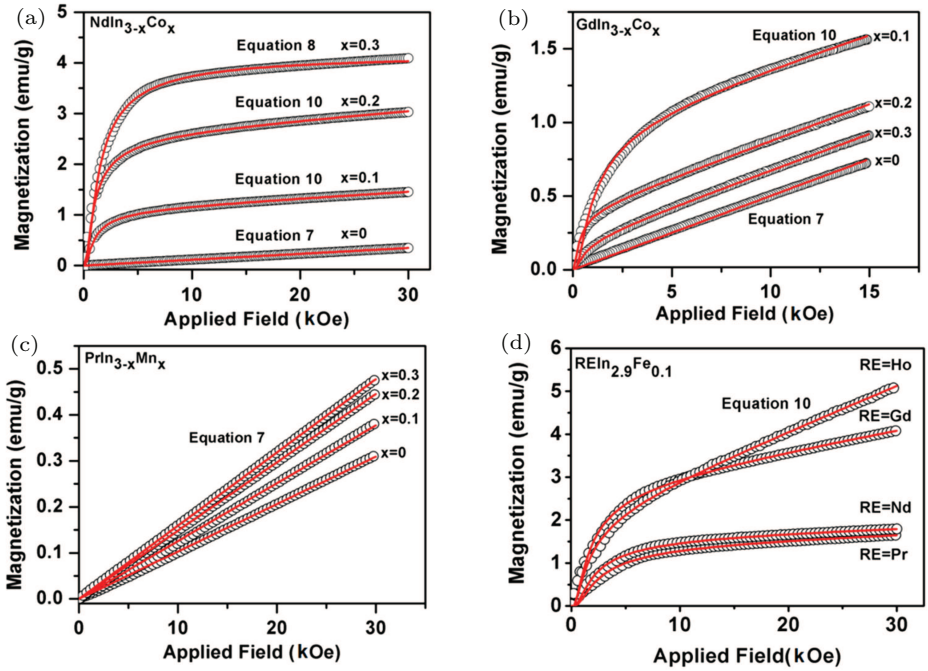


Fig. 4. The magnetizing curves of $RE\text{In}_{3-x}T_x$ at room temperature, solid lines and scatters correspond to fitting and observed results, respectively. (a) $\text{NdIn}_{3-x}\text{Co}_x$, (b) $\text{GdIn}_{3-x}\text{Co}_x$, (c) $\text{GdIn}_{3-x}\text{Mn}_x$, (d) $RE\text{In}_{2.9}\text{Fe}_{0.1}$ (RE = Pr, Nd, Gd, and Ho). The figures are adapted from Refs. [36,47,48].

The magnetic properties of $RE\text{In}_{3-x}\text{Co}_x$ are sensitive to the Co doping content. With increasing Co content in $RE\text{In}_{3-x}\text{Co}_x$, a mixture of ferromagnetic and paramagnetic phase is observed in $\text{NdIn}_{3-x}\text{Co}_x$ ($x \geq 0.2$), $\text{PrIn}_{3-x}\text{Co}_x$ ($x \geq 0.2$), respectively. The magnetic properties are strongly correlated to the phase structures. The magnetic transition from paramagnetic to ferromagnetic is caused by the phase separation of the hexagonal phase $RE\text{In}_{2-x}\text{Co}_x$ from cubic phase with increasing Co content. The saturation magnetic moment ($M_{\rm s}$) also raises with the increase of Co contents in $RE\text{In}_{3-x}\text{Co}_x$. The enhancement of magnetic moment of $RE\text{In}_{3-x}\text{Co}_x$ might be due to the partial substitution of nonmagnetic element In by 3d transition metal Co in the host material and thus a net moment is produced. The evolution of magnetic phases in $RE\text{In}_{3-x}\text{Co}_x$ might result from the exchange interaction change from the one between the isolated Co spins with the surrounding conduction electrons in Co-poor region to the one between Co–Co pairs mediated by the conduction electrons in Co-rich region.[36,38] The magnetizing behaviors of $RE\text{In}_{2.9}\text{Co}_{0.1}$ show complex magnetic prop-

erties at room temperature and follow a ferromagnetic model for RE = La and a mixed ferromagnetic and paramagnetic model for RE = Ce, Pr, Nd, Gd, Tb, Dy. The formation of ferromagnetic characteristic is suggested to result from the strong spin–spin interaction between RE and Co. It implies that Co atoms play an important role in magnetic properties of $RE\text{In}_{2.9}\text{Co}_{0.1}$.[55] The fitted and observed $RE\text{In}_{3-x}\text{Mn}_x$ exhibit paramagnetic property. The fitted susceptibility χ raises with increasing Mn contents in $RE\text{In}_{3-x}\text{Mn}_x$. Fe doping into $RE\text{In}_3$ induces the magnetic phase transition from paramagnetic to ferromagnetic. $RE\text{In}_{3-x}\text{Fe}_x$ shows a mixture of paramagnetic and ferromagnetic properties. The ferromagnetism of $RE\text{In}_{3-x}\text{Fe}_x$ is suggested to be due to 3d–3d interactions between Fe atoms and 3d–s–4f indirect interactions between Fe and rare earth atoms mediated by the conducting s electron.[47]

The electric transport of $RE\text{In}_{3-x}M_x$ is associated with its magnetic phase transition. It shows that the electric transition temperatures are very close to that of the antiferromagnetic transitions.[50] In Fig. 5, the first electric phase transition might originate from the magnetic scattering induced by the antiferromagnetic ordering at low temperature, and the other one at low temperature might be induced by the 3d–3d interaction among the unpaired 3d electron spins of Mn at face center sites in a unit cell.

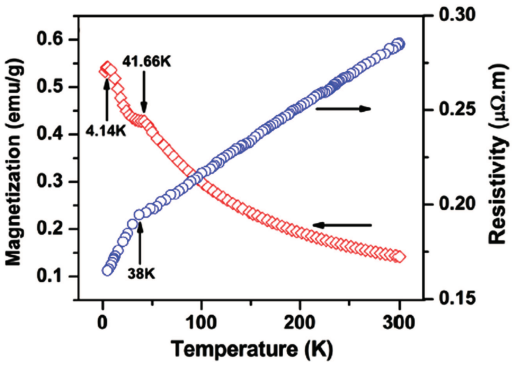


Fig. 5. The correlation of the temperature dependences of the resistivity and the magnetization for $\text{GdIn}_{2.9}\text{Mn}_{0.1}$. Reproduced with permission from Ref. [50].

A resistivity model is built for explaining the mechanism of magneto–electronic transport based on magnetic scattering at low temperature as given below:

$$\rho = \rho_0 + A\Delta^{3/2}T^{-1/2}\exp(-\Delta/T) \times \left[1+\frac{2}{3}\left(\frac{T}{\Delta}\right)+\frac{2}{15}\left(\frac{T}{\Delta}\right)^2\right], \quad (11)$$

where ρ_0 is the temperature-independent resistivity, Δ is the spin-wave gap, A is related to the spin-wave velocity.

The model works for the experimental data in the temperature range of $T < 0.6T_\text{N}$, as shown in Fig. 5. The spin-wave gap goes up with increasing Mn content and induces the increase of electric resistivity.[50] It implies that the electric transport is related to the magnon–electron scattering in the antiferromagnetic ordering state.

In the high temperature region, the Stoner spin fluctuation scattering model is listed below:

$$\rho = \rho_1 + aT^n, \quad (12)$$

where ρ_1 is the extrinsic resistivity, which is independent of the temperature. a and n are the scattering coefficient and temperature indices, respectively.

The resistivity is suggested to be originated only from the Stoner spin fluctuation in high temperature region. ρ_1 goes up with increasing Mn contents due to the magnetic scattering effect induced by the 3d–4f magnetic interaction between Mn and Gd. The aT^n term gives a good fit to the experimental data and probably originates from the phonon–electron scattering. It implies that the spin flip scattering is gradually suppressed by the phonon scattering with increasing temperature.

4. Conclusion

In this review, the studies on the structural stability and magnetic properties of dilute magnetic $RE\text{In}_{3-x}T_x$ (RE = Pr, Nd, Gd, and Ho; T = Co, Mn, and Fe) intermetallic compounds have been comprehensively summarized. Doping minor 3d transition metal Mn or Co into $RE\text{In}_3$ can still stabilize the cubic phase with a space group of $Pm\bar{3}m$. In one unit cell, the 1a crystal position is fully occupied by RE atoms and 3c crystal position is simultaneously and disorderly occupied by In and T atoms. The single-phase regions of cubic $RE\text{In}_{3-x}T_x$ correspond to the doping content x ranging from 0 to 0.3 for $RE\text{In}_{3-x}\text{Mn}_x$ and from 0 to 0.1 for $RE\text{In}_{3-x}\text{Co}_x$. Fe doping causes the decomposition of cubic phase. The structural stability of the cubic phase is suggested to be related to the effective atomic radius ratio R_A and electro-negativity difference ΔX. The metaphase $RE\text{In}_{2-x}T_x$ is separated from the cubic phase out of the single-phase solid solution region, which is formed by the rotation of the original (In, T)6 hexagonal ring driven by T partly substitution for In.

The $RE\text{In}_{3-x}T_x$ shows complex magnetic properties, which correspond to low temperature antiferromagnetic property for T = Mn and Co, room temperature ferromagnetic property for T = Co or Fe, and paramagnetic property at high temperature. The formation of the antiferromagnetic ordering might originate from the exchange interaction between the unpaired 4f electron spin of RE and the surrounding conduction electrons at low temperature. The formation of ferromagnetic characteristic is suggested to originate from the giant magnetic effect induced by doping strongly magnetic Fe or Co into $RE\text{In}_3$. The partial substitution of non-magnetic element In by strongly magnetic element in the host material through dilute dopants of T, and thus, a net moment is produced. The ferromagnetism is caused by the spin–spin interactions between

T and T or T and RE. The magnetic properties of $RE\text{In}_{3-x}T_x$ are sensitive to T content at room temperature. With the increasing contents of 3d transition metal, the magnetic phase of $RE\text{In}_{3-x}T_x$ alloys evolves from the initial paramagnetic state to an intermediated mixture of ferromagnetic and paramagnetic, and finally to ferromagnetic characteristics at room temperature.

The electric transitions are associated with magnetic transitions. The magneto-transport is suggested to be due to the electron–magnon scattering at low temperature and the Stoner spin fluctuation at high temperature.

References

[1] Molnár S V 2003 *Proc. IEEE* **91** 715
[2] Tachibana M, Taira N and Kawaji H 2011 *Solid State Commun.* **151** 1776
[3] Kaminski B, Lafrentz M, Pisarev R V, Yakovlev D R, Pavlov V V, Lukoshkin V A, Henriques A B, Springholz G, Bauer G, Abramof E, Rappl P H O and Bayer M 2010 *Phys. Rev. B* **81** 155201
[4] Mairoser T, Loder F, Melville A, Schlom D G and Schmehl A 2013 *Phys. Rev. B* **87** 014416
[5] Zhou T G, Liu Z Q and Xu Z 2012 *Chin. Phys. Lett.* **29** 047503
[6] Ahn K Y 1970 *J. Appl. Phys.* **41** 1260
[7] Boeck J D, Oesterholt R, Esch A V, Bender H and Borghs G 1996 *Appl. Phys. Lett.* **68** 2744
[8] Ohno H 1996 *Appl. Phys. Lett.* **69** 363
[9] Dietl T, Ohno H, Matsukura F, Cibert J and Ferrand D 2000 *Science* **287** 1019
[10] Twardowski A, Swiderski P, Von Ortenberg M and Pauthenet R 1984 *Solid State Commun.* **50** 509
[11] Roy V A L, Djurišić A B, Liu H, Zhang X X, Leung Y H, Xie M H, Gao J, Lui H F and Surya C 2004 *Appl. Phys. Lett.* **84** 756
[12] Ma X Y 2013 *J. Mater. Sci* **48** 2111
[13] Wang X and Ma N 2004 *J. Thermophys. Heat Transfer* **18** 476
[14] Deng Z, Zhao G Q and Jin C Q 2019 *Acta Phys. Sin.* **68** 167502 (in Chinese)
[15] Peng Y, Yu S, Zhao G Q, Li W M, Zhao J F, Cao L P, Wang X C, Liu Q Q, Zhang S J, Yu R Z, Deng Z, Zhu X H and Jin C Q 2019 *Chin. Phys. B* **28** 057501
[16] Kumar V, Sinha A, Singh B P, Sinha A P and Jha V 2015 *Chin. Phys. Lett.* **32** 127701
[17] Medvedkin G A, Ishibashi T, Nishi T, Hayata K and Sato K 2000 *Jpn. J. Appl. Phys.* **39** L949
[18] Joseph D P, Ganesan S, Kovendhan M, Suthanthiraraj S A,Maruthamuthu P and Venkateswaran C 2011 *Phys. Status Solidi A* 208 2215
[19] Guo Y Q, Li S, Wang T and Xie N N 2017 *AIP Adv.* **7** 085108
[20] Wang T, Guo Y Q, Wang C and Yang S W 2020 *J. Magn. Magn. Mater.* **502** 166506
[21] Yao J L, Kline C N, Gu H, Yan M and Aitken J A 2009 *J. Solid State Chem.* **182** 2579
[22] Yao J L, Brunetta C D and Aitken J A 2012 *J. Phys.: Condens. Matter* **24** 086006
[23] Yao J L, Rudyk B W, Brunetta C D, Knorr K B, Figore H A, Mar A and Aitken J A 2012 *Mater. Chem. Phys.* **136** 415
[24] Wang T, Guo Y Q, Wang C and Yang S W 2019 *J. Alloys Compd.* **774** 229
[25] Umehara I, Ebihara T, Nagai N, Fujimaki Y, Satoh K and Ōnuki Y 1992 *J. Phys. Soc. Jpn.* **61** 19
[26] Kletowski Z, Fabrowski R, Slawiński P and Henkie Z 1997 *J. Magn. Magn. Mater.* **166** 361
[27] Kletowski Z, Czopnik A, Tal A and De Boer F 2000 *Physica B* **281** 163
[28] Hale L, Gschneidner K A, Pecharsky V K and Mudryk Y 2009 *J. Alloys Compd.* **472** 24
[29] Kletowski Z 1992 *Solid State Commun.* **83** 241
[30] Nagai N, Umehara I, Ebihara T, Albessard A K, Sugawara H, Yamazaki T, Satoh K and Onuki Y 1993 *Physica B* **186–188** 139
[31] Bajorek A, Chełkowska G, Chrobak A and Kwiecień-Grudziecka M 2012 *Intermetallics* **26** 142
[32] Cabrera-Pasca G A, Mestnik-Filho J and Carbonari A W 2013 *J. Appl. Phys.* **113** 17
[33] Silva L S, Peixoto E B, Mercena S G, Coelho A A, Meneses C T and Duque J G S 2016 *Mater. Lett.* **175** 9
[34] Silva L S, Peixoto E B, Mercena S G, Coelho A A, Meneses C T and Duque J G S 2016 *J. Supercond. Novel Magn.* **29** 423
[35] Settai R, Kubo T, Matsuda T D, Haga Y, Onuki Y and Harima H 2006 *Physica B* **378–380** 417
[36] Han J P and Guo Y Q 2017 *Intermetallics* **89** 74
[37] Karaki Y, Kubota M, Ishimoto H and Ōnuki Y 2000 *Physica B* **284–288** 1690
[38] He Q and Guo Y Q 2016 *Appl. Phys. A: Mater. Sci. Process.* **122** 455
[39] Kletowski Z, Markowski P J and Staliński B 1986 *Solid State Commun.* **57** 293
[40] Galera R M and Morin P 1992 *J. Magn. Magn. Mater.* **116** 159
[41] He Qiang, Hanyuan L and Yongquan G 2014 *Chin. Sci. Bull.* **59** 1769
[42] Wang C, Guo Y Q and Yang S W 2019 *Chin. Phys. B* **28** 086101
[43] Guo Y Q, Grin Y, Schnelle W and Li W 2007 *J. Appl. Phys.* **101** 09N505
[44] Bittar E M, Adriano C, Giles C, Rettori C, Fisk Z and Pagliuso P G 2012 *Phys. Rev. B* **86** 125108
[45] De Negri S, Kaczorowski D, Grytsiv A, Alleno E, Giovannini M, Gorzelniak R, Rogl P, Godart C, Saccone A and Ferro R 2004 *J. Alloys Compd.* **365** 58
[46] Dhar S K, Mitra C, Manfrinetti P, Palenzona R and Palenzona A 2002 *J. Phase Equilib.* **23** 79
[47] Yang S W, Guo Y Q and Wang C 2020 *Phys. Status Solidi B* **257** 1900141
[48] Han J P and Guo Y Q 2017 *Powder Diffr.* **32** 249
[49] Liu H Y 2014 *Structure and electromagnetic transport properties of R–In–M* (R = Nd, Gd; M = Co, Mn) 1:3 intermetallic compounds, MS dissertation (Beijing: North China Electric Power University) (in Chinese)
[50] He Q, Guo Y Q and Liu H Y 2016 *J. Magn. Magn. Mater.* **401** 44
[51] He Q 2016 *Structural Stability and Dilute Magnetic Effect of Minor Co-doped Rare-Earth In-based 1:3 Compounds*, MS dissertation (Beijing: North China Electric Power University) (in Chinese)
[52] Chen S L, Guo Y Q and He Q 2015 *J. Appl. Phys.* **117** 123910
[53] Xue Z Q, Guo Y Q and Mei J 2014 *Mater. Rep.* **28** 72
[54] Keshri S, Biswas S and Wiśniewski P 2016 *J. Alloys Compd.* **656** 245
[55] Tan H and Guo Y Q 2019 *Cryst. Res. Technol.* **54** 1800228